Pathways to charge equilibration following multiple electron exchange between highly charged ions and atoms

de Nijs, Gerardus

Chapter 6

Multiple target ionization in collisions between highly charged ions and Ar

Abstract *We have performed measurements on charge state distributions of target ions produced in collisions of C^{6+}, N^{6+}, O^{6+}, Ne^{6+}, Ar^{6+} and Kr^{6+} on Ar. Charge states of Ar target ions higher than the initial projectile charge state are observed for C^{6+}, N^{6+} and O^{6+}. This intriguing observation seems to imply that even in low energy collisions ($\sim$ keV amu^{-1}) of highly charged ions on gas targets excitation of the target occurs due to inner shell electron capture. For collisions of Ar^{6+} and Kr^{6+} on Ar less than six electrons are transferred.*

6.1 Introduction

The interaction between highly charged ions and gaseous targets has received a lot of attention in the last decade. Much theoretical and experimental effort has been done to understand the dynamics of the related electron capture processes. It is now believed that one-electron capture is rather well understood (see for an overview Fritsch and Lin 1991 and references therein). Two-electron capture is more difficult to treat because of the many possibly populated states and because of electron-electron interaction (Stolterfoht *et al* 1986,1990). However, the development of the overbarrier model (Niehaus 1986) led to an intuitive understanding of the gross features of electron spectra resulting from two electron capture as observed by different groups (Mack 1987a, Bordenave-Montesquieu *et al* 1987).

It is well established that the overbarrier model predicts the band of initially populated states rather well, at least for two-electron capture. Experimental

work (e.g. Posthumus *et al* 1992, Boudjema *et al* 1989, Mack *et al* 1989, Holt *et al* 1991) as well as theoretical studies (Vaeck and Hansen 1989, Chen and Lin 1993) showed in more detail which states are populated. At the same time their investigations yielded information about energies and lifetimes of these populated states. For several collision systems the interpretation of the observed spectra led to the conclusion that after capture of electrons an unexpectedly large fraction of projectiles stabilizes radiatively (Ali *et al* 1993, Cederquist *et al* 1992a, Martin *et al* 1993, Roncin *et al* 1991). This observation has started discussions about the dynamics of stabilization after capture of electrons in excited states of the projectile (Van der Hart *et al* 1993, Kazansky and Roncin 1994, Gaboriaud *et al* 1993).

Even more complicated and less understood is the capture of electrons from many electron targets. The use of coincidence techniques (Posthumus and Morgenstern 1992) gave insight into the validity of the overbarrier model for multi-electron capture. The method also allows to study pure two-electron capture from multi-electron targets. In recent papers De Nijs *et al* (1994,1995) (chapter 4, 5) have used this technique to study pure two-electron capture processes. For an interpretation of the spectra it was necessary to assume, in view of the overbarrier model, an important contribution of three-electron processes, in which three electrons become quasi-molecular during the collision, but where the most loosely bound electron is recaptured into an excited state of the target. Although the overbarrier model in principle incorporates such target excitation processes, it was previously believed to be a minor effect (Guillemot *et al* 1990).

Measurements of the final charge state of the target can give further insight into the number of electrons transferred to the projectile. In the past many experiments were performed, in which various collision products were measured in coincidence with the charge state of selected target ions. For collisions of highly charged Xe-ions on Xe and He Cederquist *et al* (1992a) showed that the electronic structure of the projectile is of importance. Also the role of transfer excitation could be emphasized in these collisions (Cederquist *et al* 1992b). Using low energetic Ar ions extracted from a recoil ion source Cocke *et al* (1981) and Justiniano *et al* (1981) identified final charge states of both projectile and target, concluding that direct ionization of the target is negligibly small.

In this chapter we report on measurements of the final charge state of Ar after collisions with slow six-fold charged ions, done with a new high resolution charge/mass spectrometer. We studied the following process:

$$X^{6+} + Ar \rightarrow X^{(6-t)+} + Ar^{r+} + (r-t)e^{-} \qquad (6.1)$$

where X indicates one of the atoms C, N, O, Ne, Ar or Kr. The final charge state of the projectile ion is $6-t$, the charge state of the target is r so that $r-t$ electrons are emitted during or after the collision. At the low collision energies used here the emitted electrons arise mainly from autoionization processes. Due to the high resolution and sensitivity of the spectrometer it is possible to detect processes up to high $s(>5)$. The measurements indicate that the observed final charge state distributions of the target are strongly influenced by the initial

structure of the projectile core.

6.2 Experiment

Highly charged C^{6+}, N^{6+}, O^{6+}, Ne^{6+}, Ar^{6+} and Kr^{6+} ions are extracted from the ECR ion source installed at the Atomic Physics Facility at KVI, Groningen. The extraction voltage of the source has been varied from 2 to 14 kV. Isotopic ^{13}C was used to separate $^{13}C^{6+}$ from He^{2+} produced from He, which is used as mixing gas in the ECR ion source.

Downstream in the beam line a chopper is installed which yields ion beam pulses with a width of 150 ns at a frequency of 50 kHz. The voltages on the chopper plates are between -150 and 150 V.

About 2 m further the highly charged ions enter the setup, where they cross a liquid nitrogen cooled gas target. A high resolution time-of-flight mass spectrometer viewing the reaction center is mounted perpendicular to the ion beam. This reflectron type spectrometer (Mamyrin *et al* 1973) is specially designed to detect fragments from molecules after collisions with highly charged ions (Folkerts *et al* 1995). By applying a small extraction field to the reaction center, the ionized target particles can be extracted towards the detector. After a total path length of about 80 cm the ions are detected on a micro channel plate (MCP) detector.

The time-of-flight of the ions from reaction center to the MCP detector is characteristic for their m/q ratio. The flight time is measured with a time-amplitude converter which is started by the delayed chopper signal and stopped by an ion hitting the MCP detector. The digitized time-of-flights are stored using a personal computer.

During measurements the pressure in the reaction center is kept low, about 10^{-2} Pa, to avoid double collisions and the projectile ion beam current is chosen such that the number of particles in each beam burst is in the order of 10^5.

More detailed information on the experimental setup can be found in chapter 3.

6.3 Experimental results

Figure 6.1 shows charge state spectra of Ar-target ions produced by 2 keV amu^{-1} C^{6+}, Ne^{6+} and Ar^{6+} ions colliding on Ar. The horizontal axis is the time-of-flight, expressed in channel numbers, the vertical one is the observed ion yield. The ion extraction fields are chosen such that the time-of-flight for Ar^{1+} is in the order of 20μs. The observed ion yield for the lower charge states is somewhat less than the real production yield, which is a result of the extraction field in the collision center.

The detection efficiency of the higher charge states (s>2 of eq.1) is assumed to be close to 100%. This can be checked for collisions between Ar^{6+}-Ar. In figure 6.2 the relative contributions are plotted. The target-ion yields are corrected

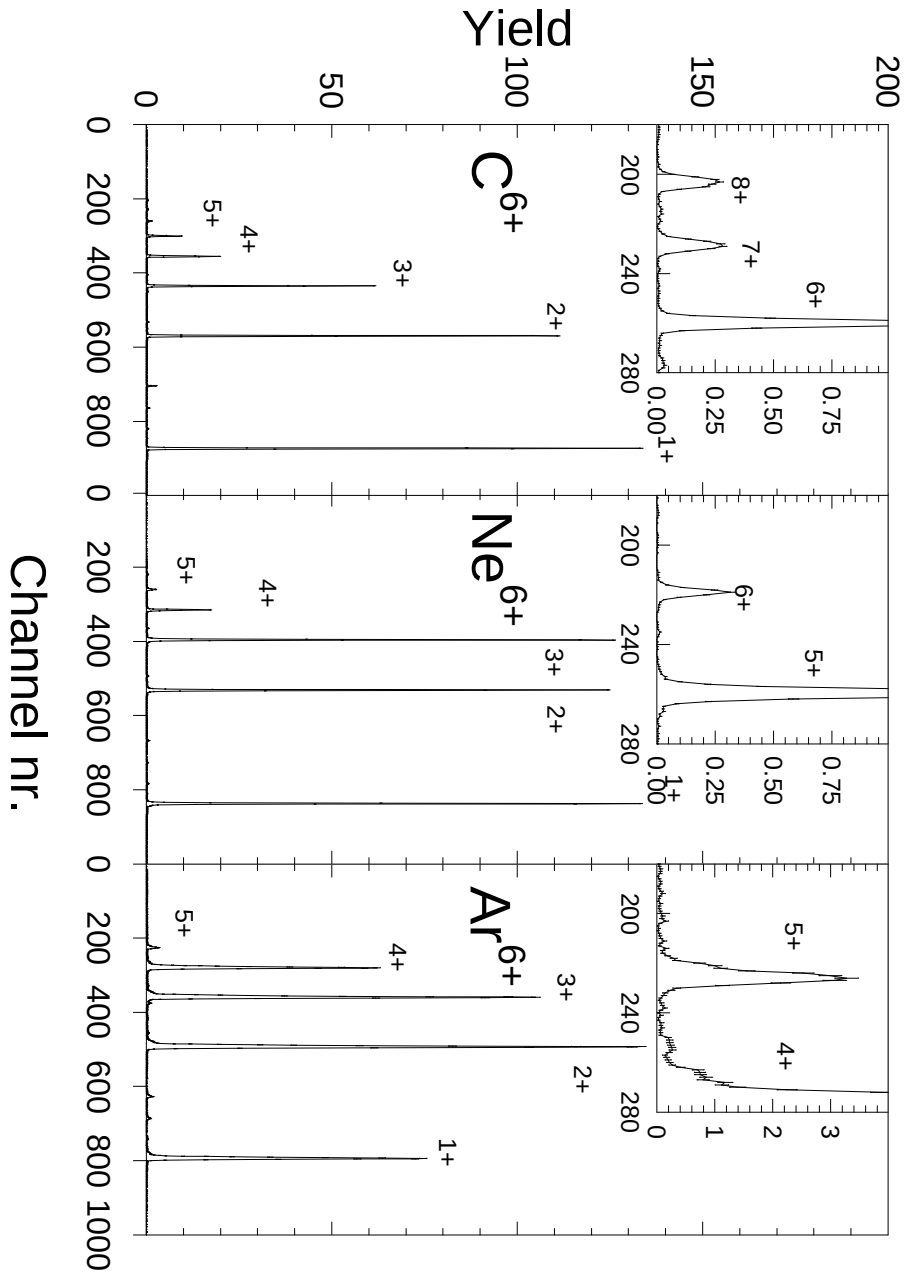

Figure 6.1: Experimental results of collisions between 2 keV amu^{-1} $^{13}C^{6+}$, Ne^{6+}, Ar^{6+} and Ar. Plotted are the charge state distribution of Ar^{q+}. The horizontal axis is the time-of-flight, expressed in channel numbers, the vertical one is the observed intensity of target-ions. In the inset of each spectrum the lower part of the spectrum is enlarged. For C^{6+} as projectile, Ar^{8+} is observed as maximum charge state. This can be explained by assuming extra autoionization of the excited Ar after capture of inner electrons (see text).

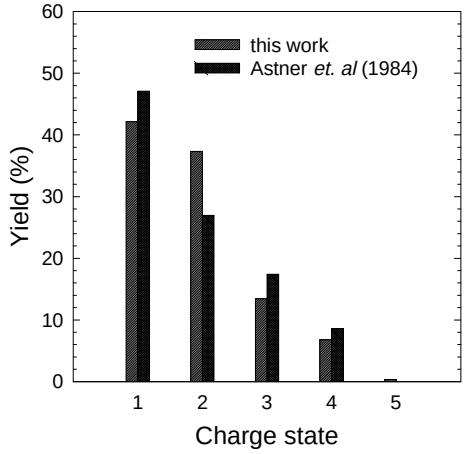

Figure 6.2: Comparison of our charge state distribution of collisions between 12 keV Ar^{6+} on Ar with the results obtained by Astner *et al* (1984).

for the relatively low extraction field in the measurements. These are compared with the work of Astner *et al* (1984). The measurements presented here are within our estimated errors of $\sim$ 20 %, in agreement with their measurements.

Peak identification is done by evaluating the peak distance relative to that of the expected charge state. The peak positions can be calculated from the linear $\sqrt{m/q}$ dependence. For all collision systems such spectra are measured and analyzed. The relative ratios of Ar^{s+} scaled to the intensity of the Ar^{3+}-intensity are summarized in figure 6.3.

Small intensities of H, N and O are also observed in the raw spectra. They result from the residual background gas pressure of 10^{-5} Pa. Not only contributions of ^{40}Ar-ions are observed but also from isotopic ^{36}Ar-ions in the expected natural abundance of a few times 10^{-4}.

6.4 Discussion

The capture of electrons from atoms into highly excited states of the projectile ions can be described with the overbarrier model (Niehaus 1986, chapter 2). The model predicts binding energies, principal quantum numbers and cross sections for the different electron capture processes. Furthermore it provides reaction windows. These Gaussian shaped windows define the binding energy range around the calculated central binding energy. In this range capture is presumed to take place. The width of a reaction window is proportional to the square root of the collision velocity.

During ion-atom collisions a quasi-molecule is formed. Each electron in the target sees a potential barrier formed due to the extra potential of the projectile. On the way-in the height of the barrier decreases as the internuclear distance

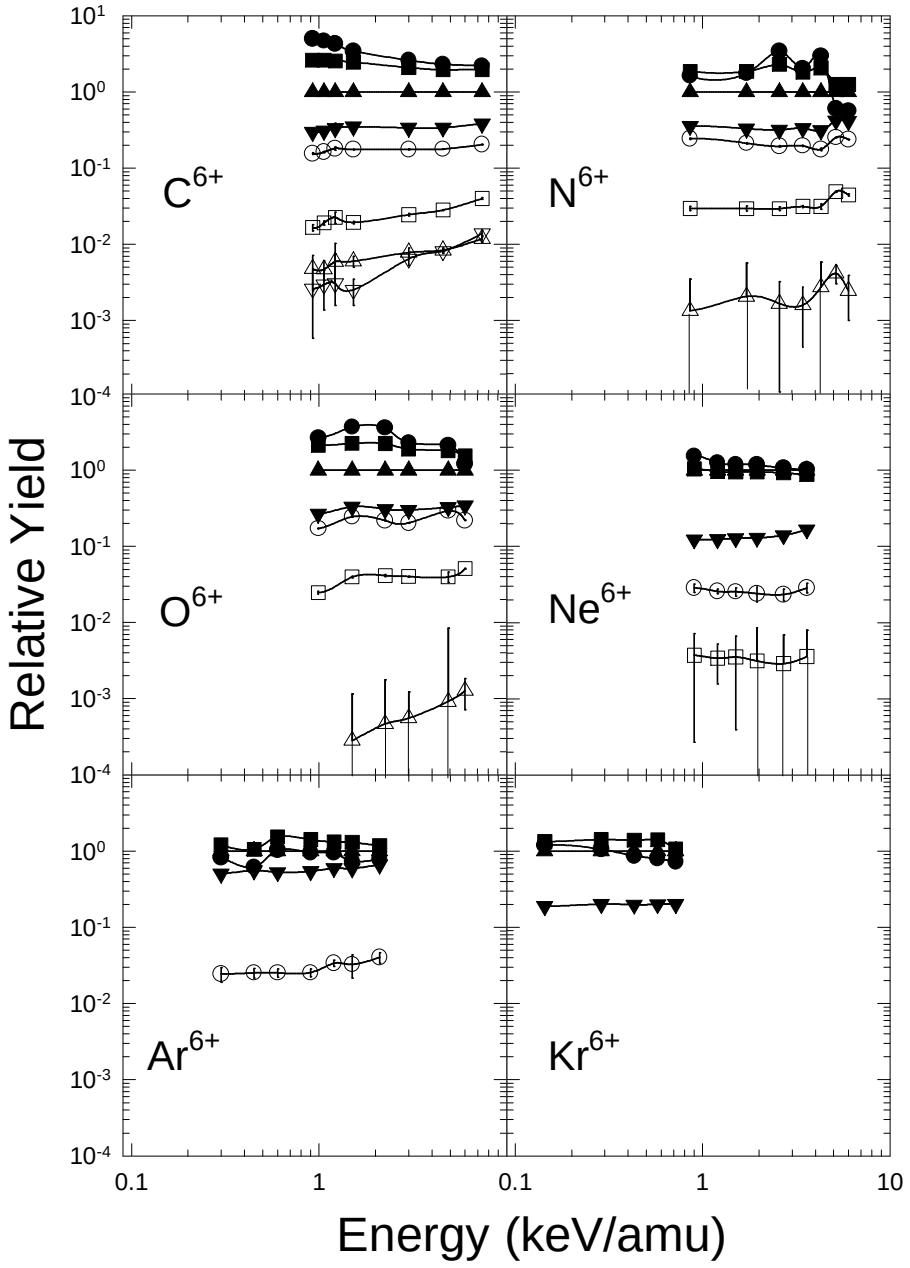

Figure 6.3: The observed relative yield of distributions of Ar^{s+} as function of the collision energy for different 6+ projectiles, normalized to Ar^{3+}. The different symbols indicate the charge state of the target: closed symbols ○ 1+, □ 2+, △ 3+, ▽ 4+, and the open symbols ○ 5+, □ 6+, △ 7+, ▽ 8+. From this figure it is clear that the final charge state depends on the electronic structure of the six-fold ionized projectiles.

decreases. Once the barrier height equals the binding energy of an electron it is not localized anymore on the target, but has become quasi-molecular. After having reached the point of closest approach the ions start to recede and the potential barrier between the ions increases again. At the point at which the barrier height reaches the quasi-molecular energy of the electron, the electron will be captured either by the projectile or by the target.

The actual orbital energies of the captured electrons lie inside the previously described reaction windows. The binding energies of the stationary ionic states at infinite nuclear distance are calculated with self-consistent Hartree-Fock calculations using the Cowan-code (Cowan 1981).

projectile	configuration	average BE (eV)	Ar^{q+} max
C^{6+}		490	8+
N^{6+}	(1s)	552	7+
O^{6+}	$(1s^2)$ /(1s2s)	132/693	7+
Ne^{6+}	$(1s^22s^2)$	158	6+
Ar^{6+}	(core)$(3s^2)$	94	5+
Kr^{6+}	(core)$(4s^2)$	75	4+

Table 6.1: Summary of average binding energies for the lowest lying unoccupied orbitals of the various projectiles with their configurations. Also tabulated are the maximum observed charge states of Ar. From this table it is clear that the initial configuration and binding energy strongly influences the maximum charge state of the target.

In table 6.1 we summarize configurations and average binding energies of the lowest lying unoccupied orbitals of the projectiles and the measured maximum target charge state, resulting from collisions with Ar.

Apparently there is a significant difference between projectiles with and without primary K-shell vacancies: those with such vacancies give rise to final target charge state higher than the primary projectile charge, whereas those without do not. Since the maximum observed charge state of Ar seems to be dependent on this distinction we will discuss them accordingly. In 6.4.1 the collisions between C^{6+}, N^{6+}, and metastable O^{6+} on Ar will be discussed and in 6.4.2 the collisions between O^{6+}, Ne^{6+}, Ar^{6+} and Kr^{6+} on Ar.

6.4.1 Projectiles with K-shell vacancies: C^{6+}, N^{6+} and metastable O^{6+}+ Ar

If we examine the different charge states of Ar formed by the collisions between C^{6+} and Ar, plotted in figure 6.1, we observe besides the large contributions of Ar^{1+} to Ar^{4+}, also contributions of Ar^{5+} up to Ar^{8+}. The formation of Ar^{7+} and Ar^{8+} is in the first place unexpected since their charge states exceed the charge state of the projectile, C^{6+}. The observation of these ions indicates that during or after the collision electrons are ejected from the target. Direct

ionization of the target is negligible in this collision energy range (Cocke *et al* 1981, Justiniano *et al* 1981). To explain the increase of the final charge state we have to assume production of excited target ions, which subsequently autoionize, thereby increasing their charge state.

In view of the various binding energies involved it is very likely that such excited target ions are created via transfer of inner-shell electrons from the target to the projectile. Binding energies of 1s-electron vacancies in C^{6+} and C^{5+} are 490 and 392 eV respectively, which is in the same range as ionization energies of the least bound Ar L-shell electrons (420-915 eV). Therefore electron transfer from the L-shell of Ar to the K-shell of C is very likely. Two subsequent autoionization steps in which the Ar-L-shell is filled can lead to an increase of the target charge state from q to q+2.

For high energy collisions (MeV) inner shell electron transfer processes have been studied extensively (see e.g. Hagmann *et al* 1986, Schlachter *et al* 1989, Stolterfoht 1987).

From such a transfer of inner shell electrons one can also try to understand the experimentally observed dependence of the cross sections on the collision velocity: for an effective electron transfer between argon L-shell and carbon K-shell impact parameters in the order of the argon L-shell radius are required. Besides a correspondingly small cross section this also implies that the collision energy has to be sufficiently high to overcome the Coulomb repulsion of the colliding partners, which becomes active when a large number of electrons (here up to 8) have become quasi-molecular and do not longer shield the nuclear charges. In figure 6.5 we plot the dependence of the Ar^{8+} and the Ar^{7+} yield - normalized to the Ar^{1+} yield - as a function of the collision energy. The velocity dependence due to the Coulomb repulsion mentioned above is shown as the dotted line. To obtain this line impact parameter dependent classical trajectories were calculated, along this trajectory the effective nuclear charge on the way in is stepwise increased when additional electrons become quasi-molecular. On the way out the effective charges are changed depending on capture or recapture of electrons. Clearly the measured velocity dependence is much more pronounced than expected from the dotted line.

From the overbarrier model we can deduce an extra velocity dependence. The width ΔE of a reaction window for an electron, centered around the effective binding energy, is a function of the collision velocity (Niehaus 1986):

$$\Delta E = \sqrt{v_{rad}\frac{dV}{dt}} \tag{6.2}$$

with v_{rad} the radial velocity and $\frac{dV}{dt}$ the derivative of the potential barrier at the capture distance. The shape of the reaction window is assumed to be Gaussian. A measure for the probability to capture an electron can be deduced from the weighted energy separation between available levels. The probability can be estimated from the reaction windows by assuming that it is proportional to the relative height of the window at the available levels.

The probability P to capture of the $n-th$ electron (n=1 is the outer, most

loosely bound electron, n=2 the next electron etc.) into the projectile is then given by

$$P = \exp(-\frac{(E_{qm} - E_p)^2}{2\Delta E^2}) * [\exp(-\frac{(E_{qm} - E_p)^2}{2\Delta E^2}) + \exp(-\frac{(E_{qm} - E_t)^2}{2\Delta E^2})]^{-1} \quad (6.3)$$

where E_{qm} is the quasi-molecular binding energy calculated with the overbarrier model. E_t and E_p are the binding energies of the electron in the target and projectile respectively, but calculated at the distance where the capture takes place introducing a shift q/R_c in the binding energy. For the target electrons $q = 6$ is used, for the electrons captured into projectile levels $q = 9$ for the 9th and $q = 10$ for 10th electron is used.

For the formation of Ar^{8+} two L-shell vacancies have to be created. For the probability $P_{Ar^{8+}}$ all possible capture processes have to be taken into account. The necessary condition is that the 10th as well as the 9th electron are captured by the projectile and moreover four of the eight M-shell electrons. Therefore $P_{Ar^{8+}}$ is estimated to be

$$P_{Ar^{8+}} = P_{10} * P_9 * (\Sigma_\sigma \Pi_{i=1}^{8} P_i^\sigma) \quad (6.4)$$

with Σ_σ indicating a sum over all the different possible strings σ, i.e. the different possible combinations to capture or to recapture an electron. The product term Π indicates the probability to capture the remaining electrons in the string σ. The probabilities P_i are calculated with respect to possibly previously captured electrons, so maintaining the string characteristic.

The target binding energy of the 10th electron in Ar at 1.45 a.u. is 591 eV, the energy of the lowest orbital in C^{6+} is 678 eV. The width of the reaction window is 56 eV for a collision energy of 60 keV. For recapture into the target the binding energy of the available orbital is equal to the quasi-molecular energy of 591 eV. This situation is shown in figure 6.4 for collisions between C^{6+} and Ar. Drawn are the potential wells seen by an electron in the quasi-molecule at the point on the outgoing path where the electron will be captured or recaptured. In this figure also the reaction windows are shown for two energies. In the reaction windows the energies of those orbitals are plotted into which the electron will be captured or recaptured. The energy dependence for the 10th electron is stronger than that for the 9th electron in Ar.

For the formation of Ar^{7+} the situation is a bit more complicated. In this case it is necessary to incorporate the possibility to capture either the 9th *or* the 10th electron, in each case yielding an L-shell vacancy, the necessary condition for creation of Ar^{7+}. The probability $P_{Ar^{7+}}$ is thus

$$P_{Ar^{7+}} = [P_{10} * (1 - P_9) + P_9^* * (1 - P_{10}) + P_9^*] * (\Sigma_\sigma \Pi_{i=1}^{8} P_i^\sigma) \quad (6.5)$$

The first two terms in the formula indicate the case where ten electrons have become quasi-molecular. For the possibility of nine quasi-molecular electrons,

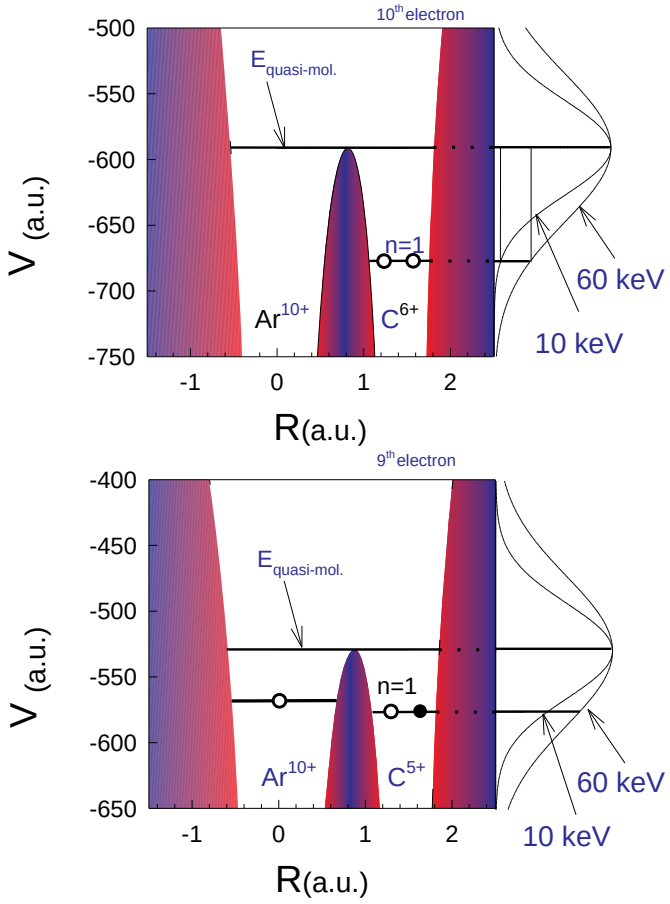

Figure 6.4: Potential energies as seen from the 10th electron (upper panel) and the 9th electron (lower panel) of Ar for collisions between C^{6+} and Ar at the point where on the outgoing path of the collision the electron will be captured or recaptured. Indicated as $E_{quasi-mol}$ is the quasi-molecular energy of the electron. Also drawn are the nearest available orbitals in the projectile and target. For electron 10 the target states coincide with the quasi-molecular energy. The figure for the 9th electron is drawn for the case that the 10th electron has been captured by the projectile. On the right side the reaction windows are drawn for two collision energies.

i.e. somewhat larger impact parameters, the last term is included. The P_9 term is the probability of capturing an electron when the 10th electron is already captured. The P_9^* is for the case that the 10th electron is *recaptured* by the target. This difference is important for the shift due to the induced Coulomb field of the collision partners. For P_9 the 9th electron is shifted in the field of a 5+ core, where for P_9^* this electron is shifted in the field of the original 6+ core.

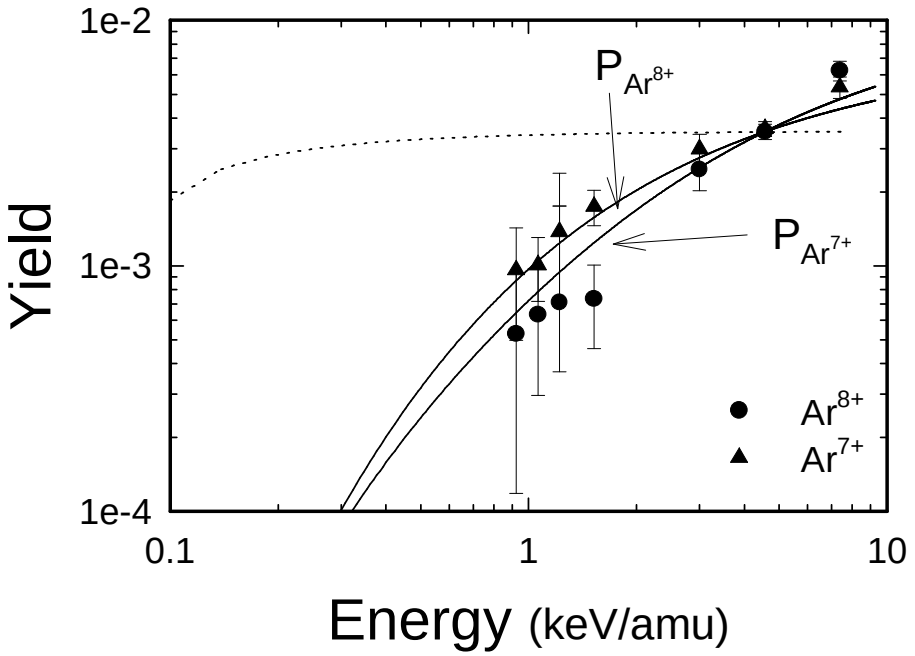

Figure 6.5: Velocity dependence of intensity of Ar^{8+} and Ar^{7+} in collisions between C^{6+}. The dotted line is the expected ratio calculated from classical trajectory using only Coulomb repulsion between the projectile and target in the quasi-molecule. The solid lines stems from calculations where the velocity dependent width of the reaction window determines the probability of capture into the projectile or target (see text).

In figure 6.5 we plot $P_{Ar^{q+}}$ as function of the collision energy. As a first approximation the sum terms in the formulae are taken to be constant over the collision energy, because no strong velocity dependence of the relative yield is observed for the collision systems where only M-shell electron capture is expected. We observe that this approach describes the observed velocity dependence at least qualitatively. A precise calculation would have to include all the different strings weighted with the appropriate recapture distances. In the calculations this distance was chosen about 1.5 a.u. for both 9th and 10th electron.

To summarize, in view of the fact that the two 1s-vacancies in C^{6+} are nearly resonant with the Ar L-shell it is believed that filling of these two vacancies creates two L-shell vacancies in Ar. The resulting highly excited target may subsequently autoionize two times to fill the Ar L-shell vacancies. This

mechanism can be tested by comparing with projectiles containing only one or even no K-vacancies, resonant with the Ar L-shell. To exemplify this we plotted in figure 6.6 the ionization energies of electrons in the orbitals of various 5+ ions compared to the ionization energies of Ar. So for N^{6+} with one vacancy in resonance with the L-shell of Ar an increase of the target charge state of 1 is expected.

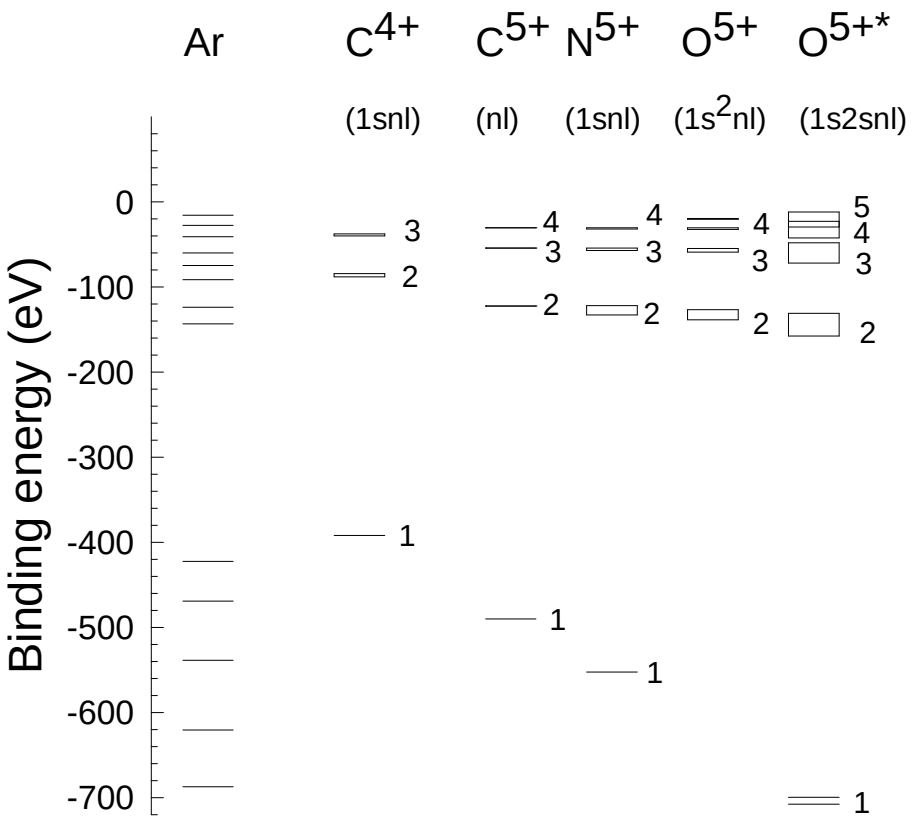

Figure 6.6: Energy level diagram for C^{4+}, C^{5+}, N^{5+}, O^{5+} and metastable O^{5+}, indicated with *, and ionization energies of Ar. The binding energy of the n=1 electrons in the various ions is comparable to the ionization energy of the L-shell in Ar. From this picture it is clear that there is a possibility for capture from L-shell electrons into the n=1 shells of different projectiles, creating vacancies in the L-shell of Ar.

The orbital energy of the K-shell vacancy in N^{6+} is 540 eV, which is close to the L-shell electrons of Ar, with ionization energies ranging between 420 and 915 eV. This implies that an electron from the L-shell of Ar can in principle be captured quasi-resonantly into the K-shell vacancy in N^{6+}. The resulting L-shell vacancy in Ar can decay via autoionization thus yielding a maximum Ar charge state of 7+. A similar situation exists for metastable O^{6+}. In ion beams created with ECR-sources a considerable fraction (5$\sim$10%) of the beam consists

of metastable O^{6+} with configuration (1s2s) (Mack 1987b). The 1s-ionization energy of $O^{5+}(1s^22s)$ is 693 eV, resonant with Ar L-shell. In our opinion the observed Ar^{7+} is due to capture of electrons into 1s-orbital of metastable O^{6+}.

O^{6+} in the ground state has no K-vacancies. It is therefore expected that the maximum charge state of Ar will not exceed the maximum projectile charge state. We will discuss this in the following sub-section.

6.4.2 Projectiles with filled K- or L-shells: O^{6+}, Ne^{6+}, Ar^{6+} and Kr^{6+} + Ar

When projectiles with filled inner-shell orbitals are used a direct electron exchange between inner projectile- and target-orbitals is impossible. Therefore one expects that for such projectiles autoionization processes in the target subsequent to the collision do not take place, and that consequently the maximum target charge state does not exceed the initial projectile charge state. From figure 6.1 one can see that this expectation is generally justified.

When going from Ne^{6+} via Ar^{6+} to Kr^{6+} projectiles we observe maximum charge states of the Ar target of q=6, q=5 and q=4 respectively. One might wonder why not in all three cases up to 6 electrons are transferred. To some extent the binding energies involved are responsible for this: whereas transfer of a total of 6 electrons from Ar to the Ne^{6+} projectile can occur as an exothermic process, a similar transfer to the Kr^{6+} projectile is an endothermic process and thus less likely. Just to give an indication of this: ionization potentials of Ne^{5+}, Ar^{5+} and Kr^{5+} are 158 eV, 94 eV and 75 eV respectively. For Ar^{6+} collisions on Ar a transfer of 6 electrons can in principle take place near resonantly (apart from a change in translational electronic energy). However here another aspect becomes important: in the classical overbarrier model it is always presumed that the highly ionized projectile contributes non-occupied atomic orbitals to the formation of quasi-molecular orbitals during the collision. As long as bare projectile ions are used this assumption is justified. For a symmetric many-electron system like Ar^{6+} + Ar however electron promotion during the approach of the collision partners has to be taken into account. This implies that inner shell projectile electrons have to be accommodated in the quasi-molecular orbitals, thus inhibiting a quasi resonant transition of many electrons. Although a simultaneous transition of all 6 electrons is no doubt a near resonant process, a one-by-one transfer of electrons is not necessarily a resonant process for every step. In view of the electron promotion it is therefore not amazing that during Ar^{6+} on Ar collisions a transfer of 6 electrons turns out to have a cross section below our detection limit, implying that it is at least four orders of magnitude smaller than the cross section for three-electron transfer.

The aspect of electron promotion is certainly also important on Kr^{6+} on Ar collisions, and to a large extent responsible for the fact that a transfer of at most 4 electrons is observed. This implies that the classical overbarrier model can not simply be applied to collision systems with filled inner shells even if one of the collision partners is highly ionized.

6.5 Conclusions

We have performed charge state distribution measurements for collisions between various highly charged ions and Ar, using a new high resolution spectrometer. An unexpectedly high charge state - higher than the projectile charge state - was observed for C^{6+} and N^{6+} projectiles. We ascribe this to autoionization of the target after capture of inner shell electrons from Ar. This is direct evidence for the formation of strongly excited target ions resulting from capture processes, which was already invoked by De Nijs *et al* (1994, 1995) to interpret energy spectra of projectile emitted electrons.

For Ar^{6+} and Kr^{6+} projectiles on the other hand unexpectedly low target charge states have been observed (always less than the projectile charge). We ascribe this to the presence of many inner-shell electrons which are promoted during the collisional formation of the quasi-molecule. Such a promotion results in occupied orbitals and thus inhibits an effective capture of electrons. For such systems with many inner-shell electrons the classical overbarrier model can not longer be applied without great care. A more detailed interpretation would require the knowledge of quantitative correlation diagrams and potential energy curves.

Acknowledgments

We would like to thank Stefan Schippers for kindly helping out with the Hartree-Fock calculations.

References

Ali R, Cocke C L, Raphaelian M L A and Stöckli M 1993 *J. Phys. B: At. Mol. Opt. Phys.* **26** L177

Astner G, Bárány A, Cederquist H, Danared H, Huldt S, Hvelplund P, Johnson A, Knudsen H, Liljeby L and Rensfelt K G 1984 *J. Phys. B: At. Mol. Phys.* **17** L877

Bordenave-Montesquieu B, Benoit-Cattin P, Boudjema M, Gleizes A and Dousson S 1987 *Nucl. Instrum. Methods* B **23** 94

Cederquist H, Andersson H, Beebe E, Biedermann C, Broström L, Engström Å, Gao H, Hutton R, Levin J C, Liljeby L, Pajek M, Quinteros T, Selberg N and Sigray P 1992a *Phys. Rev.* A **46** 2592

Cederquist H, Beebe E, Biedermann C, Engström Å, Gao H, Hutton R, Levin J C, Liljeby L, Quinteros T, Selberg N and Sigray P 1992b *J. Phys. B: At. Mol. Opt. Phys.* **25** L69

Chen Z and Lin C D 1993 *Phys. Rev.* A **48** 1298

Cocke C L, DuBois R, Gray T J, Justiniano E and Can C 1981 *Phys. Rev. Lett.* **46** 1671

Cowan R D 1981 *The Theory of Atomic Structure and Spectra* (Berkeley, CA: University of California Press)

Folkerts H O, Bliek F W, De Jong M, Hoekstra R and Morgenstern R 1995 *Nucl. Instrum. Methods* B **98** 389

Fritsch W and Lin C D 1991 *Phys.Rep.* **202** 1&2 1

Gaboriaud M N, Roncin P and Barat M 1993 *J. Phys. B: At. Mol. Opt. Phys.* **26** L303

Guillemot L, Roncin P, Gaboriaud M N, Laurent H and Barat M 1990 *J. Phys. B: At. Mol. Opt. Phys.* **23** 4293

Hagmann S, Kelbch S, Cocke C L, Richard P, Skutlartz A, Schmidt-Böcking H, Schuch R, Johnson B, Meron M and Jones K 1986 *Phys. Rev.* A **34** 2897
Van der Hart H W and Hansen J E 1993 *J. Phys. B: At. Mol. Opt. Phys.* **26** 641
Holt R A, Prior M H, Randall K L, Hutton R, McDonald J and Schneider D 1991 *Phys. Rev.* A **43** 607
Justiniano E, Cocke C L, Gray T J, DuBois R D and Can C 1981 *Phys. Rev.* A **24** 2953
Kazansky A K and Roncin P 1994 *J. Phys. B: At. Mol. Opt. Phys.* **27** 5537
Mack M 1987a *Nucl. Instrum. Methods* B **23** 74
Mack M 1987b *thesis* Rijksuniversiteit Utrecht, Netherlands
Mack M, Nijland J H, Van der Straten P, Niehaus A and Morgenstern R 1989 *Phys. Rev.* A **39** 3846
Mamyrin B A, Karataev V I, Shmikk D A and Zagulin V A 1973 *Sov.Phys. JETP* **37** 45
Martin S, Denis A, Delon A, Désesquelles J and Ouerdane Y 1993 *Phys. Rev.* A **48** 1171
Niehaus A*J. Phys. B: At. Mol. Phys.* **19** (1986) 2925
De Nijs G, Hoekstra R and Morgenstern R 1994 *J. Phys. B: At. Mol. Opt. Phys.* **27** 2557
De Nijs G, Hoekstra R and Morgenstern R 1995 *Nucl. Instrum. Methods* B **98** 307
Posthumus J H, Lukey P and Morgenstern R 1992 *J. Phys. B: At. Mol. Opt. Phys.* **25** 987
Posthumus J H and Morgenstern R 1992 *J. Phys. B: At. Mol. Opt. Phys.* **25** 4533
Raphaelian M L A, Berry H G, Berrah N and Schneider D 1993 *Phys. Rev.* A **48** 1292
Roncin P, Gaboriaud M N and Barat M 1991 *Europhys. Lett.* **16** 551
Schlachter A S, Stearns J W, Berkner K H, Bernstein E M, Clark M W, DuBois R D, Graham W G, Morgan T J, Mueller D W, Stöckli M P, Tanis J A and Woodland W T 1989 *Nucl. Instrum. Methods* B **40/41** 21
Stolterfoht N 1987 *Progress in Atomic Spectroscopy, part D* ed. H.J. Beyer and Hans Kleinpoppen (Plenum Publishing Corporation)
Stolterfoht N, Sommer K, Swenson J K, Havener C C and Meyer F W 1990 *Phys. Rev.* A **42** 5396
Stolterfoht N, Havener C C, Phaneuf R A, Swenson J K, Shafroth S M and Meyer F W 1986 *Phys. Rev. Lett.* **57** 74
Vaeck N and Hansen J E 1989 *J. Phys. B: At. Mol. Opt. Phys.* **22** 3137